Evaluation of Foundation Stiffness of Tower B2 at the Block Island Wind Farm

BSEE Project Report

Contract Number 140E0119C0003

Aaron Bradshaw[1]

Maeve Story[2]

1 Professor, Department of Civil and Environmental Engineering, University Rhode Island, Kingston, RI 02881

2 Graduate Student, Department of Ocean Engineering, University Rhode Island, Narragansett, RI 02882

June 2022

TABLE OF CONTENTS

1.0 EXECUTIVE SUMMARY

The objective of this task was to estimate the foundation stiffness (i.e., spring constants) for dynamic structural modeling of the Block Island Wind Farm jacket structure. Static pushover analyses were performed on a model of a single jacket pile using the Winkler (i.e., t-z or p-y) approach, which is commonly used in engineering practice. Non-linear load-displacement curves (i.e., "backbone" curves) were developed for both vertical and lateral loading. The vertical load-displacement curves were also used to define a range of vertical foundation spring constants within the anticipated service load ranges.

2.0 BACKGROUND

Structural finite element models have been developed for Turbine B-2 that include the major structural components of the system including the foundation, jacket, transition piece, tower, and nacelle. In these models each pile will be represented as a 'super-element' consisting of a six-degree-of-freedom stiffness matrix placed at a node at the bottom of each jacket leg at the mudline level. Preliminary dynamic analysis by Tufts suggested that the first bending mode of vibration (both fore-aft and side-to-side motions) is most sensitive to the vertical foundation stiffness. The lateral stiffness could also be important for the torsional modes that occur at higher vibration frequencies. The objective was to estimate the stiffness of the BIWF foundation piles in both the vertical and lateral directions. The remaining subsections describe the pushover analysis methodology and results as well as an interpretation of the range of vertical foundation spring constants.

3.0 FOUNDATION PUSHOVER ANALYSIS METHODOLOGY

The stiffness of the pile-soil system was assessed using a Winkler approach, in which the pile is modeled as a beam and the soil as a series of very closely spaced non-linear springs. This method is considered the standard of practice for the analysis of jacket structures (e.g., Mostafa and El Naggar 2004; Abhinav and Saha 2018). It was also the methodology used by the design geotechnical engineer for the BIWF piles. The 't-z' and 'q-z' curves describe the stiffness of the frictional and end bearing soil springs, respectively. The 'p-y' curves describe the stiffness of the lateral soil springs. Since the pile is battered, application of the vertical load will engage both

the axial and lateral soil springs. Therefore, it was necessary in this study to specify t-z, q-z, and p-y curves. The modeling was performed using RSPile software developed by Rocscience.

3.1 Properties of the BIWF Piles

The BIWF jacket structures consist of four legs, each inclined at a batter angle of 4.24V:1H. The pipe piles that support the jacket were driven through the inside of the tubular steel jacket legs. The piles have a diameter of 1,524 mm and a wall thickness 44.45 mm. The piles at Turbine B2 were driven to embedment depths of 51.8 to 54.4 m below the seafloor.

Foundation stiffness and capacity can be affected by scour because of the removal of soil from around the pile. The platform owner has been monitoring scour at the platforms and indicate relatively small changes in the mudline elevation (< ~20 cm) since installation. Therefore, the analysis presented herein assumes that there is no scour or sediment accumulation around the jacket legs.

3.2 Idealized Soil Profile

The original BIWF project considered seven turbine locations and thus one geotechnical boring was performed at each of the seven locations. The geotechnical engineer who conducted the site investigations developed idealized soil profiles for each of the seven borings including properties for the analysis of pile capacity and lateral deflection. The analysis presented herein used the idealized soil profile developed for Boring B-5 that is at the same location as Turbine B2. The idealized profile is summarized in Table 1 and indicates that the subsurface conditions consist mainly of sand.

Table 1. Idealized soil profile for Boring B-5 presented in the site investigations report.

Depth Below Existing Mudline	Soil Type	Total Unit Weight	Remolded Shear Strength	Intact Shear Strength	Soil Friction Angle	Interface Friction Angle	K	N_q	Max Side Friction	Max End Bearing	ε_{50}	K_s	K_c
m		kN/m^3	kPa	kPa	deg	deg			kPa	kPa		kN/m^3	kN/m^3
0			-	-									
11.0	Sand	19.9	-	-	34	27	0.8	30	86	7200	-	20	
11.0			27	96									
24.1	Stiff Clay	18.0	64	96	-				48	-	0.003	136	54
24.1			-	-									
32.9	Sand	21.0	-	-	34	27	0.8	30	86	7200	-	20	
32.9			-	-									
40.2	Sand	17.8	-	-	34	27	0.8	30	86	7200	-	20	
40.2			-	-									
47.6	Sand	21.0	-	-	34	27	0.8	30	86	7200	-	20	
47.6			67	96									
48.8	Stiff Clay	17.8	67	96	-				48	-	0.003	136	54
48.8			-	-									
52.7	Sand	21.0	-	-	34	27	0.8	30	86	7200	-	20	
52.7			-	-									
53.0	Sand	21.0	-	-	34	27	1	30	86	7200	-	20	

Cone Penetration Testing (CPT) was also performed as part of the site investigations by pushing a cone in at the bottom of the borehole in 6-meter intervals. As part of the current study, the CPT data were used to estimate pile capacity as well as the small strain modulus of the soil (G_0) which is important for estimating the foundation stiffness at low load levels. Table 2 summarizes representative properties of cone tip resistance and G_0 for each of the idealized soil profile layers. The empirical correlations that were used to obtain G_0 are summarized below.

Quartz Sand (Rix and Stokoe 1991):

$$G_0 = 1634\left(q_c\right)^{0.25}\sigma'_v{}^{0.375} \quad (1)$$

Clay (Mayne and Rix 1993):

$$G_0 = 406\left(q_c\right)^{0.695}e^{-1.13} \quad (2)$$

where G_0=small strain shear modulus in kPa, q_c=cone tip resistance in kPa, σ'_v=vertical effective stress in kPa, and e=void ratio. The void ratio of the clay layers was estimated from the water content (w) and specific gravity (G_S) data provided in the site investigations report.

Table 2. Additional soil properties that were assessed at Boring B-5 as part of this study.

Depth Below Existing Mudline	Soil Type	Cone Tip Resistance	D_{50}	Constant Volume Interface Friction Angle	Water Content	G_s	e_0	G_0
m		MPa	mm	deg	%			MPa
0.0								
11.0	Sand	20*	0.17	29	-	-	-	88
11.0								
24.1	Stiff Clay	6	-	-	29	2.74	0.79	224
24.1								
32.9	Sand	20	0.17	29	-	-	-	158
32.9								
40.2	Sand	24	0.17	29	-	-	-	182
40.2								
47.6	Sand	20	0.17	29	-	-	-	187
47.6								
48.8	Stiff Clay	6	-	-	34	2.74	0.93	186
48.8								
52.7	Sand	23	0.17	29	-	-	-	205
52.7								
53.0	Sand	28	0.17	29	-	-	-	219

Note: *Assessed from adjacent borings

3.3 Ultimate Shaft and End-Bearing Capacities

The t-z portion of the analysis requires an estimate of both the ultimate unit shaft resistance and the ultimate unit end-bearing resistance, which establishes the maximum resistance in the t-z relationships both in compression and tension. Consistent with the geotechnical consultant's preliminary pile capacity calculations, the API method commonly called the "API Main Text" method was used to calculate the ultimate axial capacity. This includes the "beta" method for sand layers and the "alpha" method for clay layers. Consistent with the original design recommendations a shaft resistance reduction factor of 0.8 was applied to the tensile loading case to account for Poisson's effect.

As part of this study, the pile capacity was also assessed using the "offshore" UWA-05 method for sand. The procedure and equations are given in Lehane (2005) and in the appendix of the API code. This method is one of the five available state-of-the-art methods proposed for offshore pile design that is based of the Cone Penetration Test (CPT). All of these methods are summarized in the appendix of the API code. The main advantages of the CPT-based methods are that they are believed to more accurately represent the mechanics around the pile, including the lateral stresses

on the pile and cyclic reduction in frictional capacity (i.e. friction fatigue) that occurs as a result of pile driving.

Static capacity models for sands are typically calibrated from pile loads tests that are performed with a week or so of installation. The BIWF platforms were put in service in December 2016 and thus will have been in service for about 4 years by the start of the health monitoring campaign. Research has shown that axial pile capacity in sands significantly increases within about the first 200 days after installation as shown in Figure 1. Ageing effects were also observed in reduced scale piles in sands that were tested as part of a recent research project also funded by BOEM (Rahim et al. 2020). Therefore, the effects of ageing were considered in one of the analysis cases discussed later. In this case it was assumed that the pile capacity has doubled from ageing based on the trends in Figure 1.

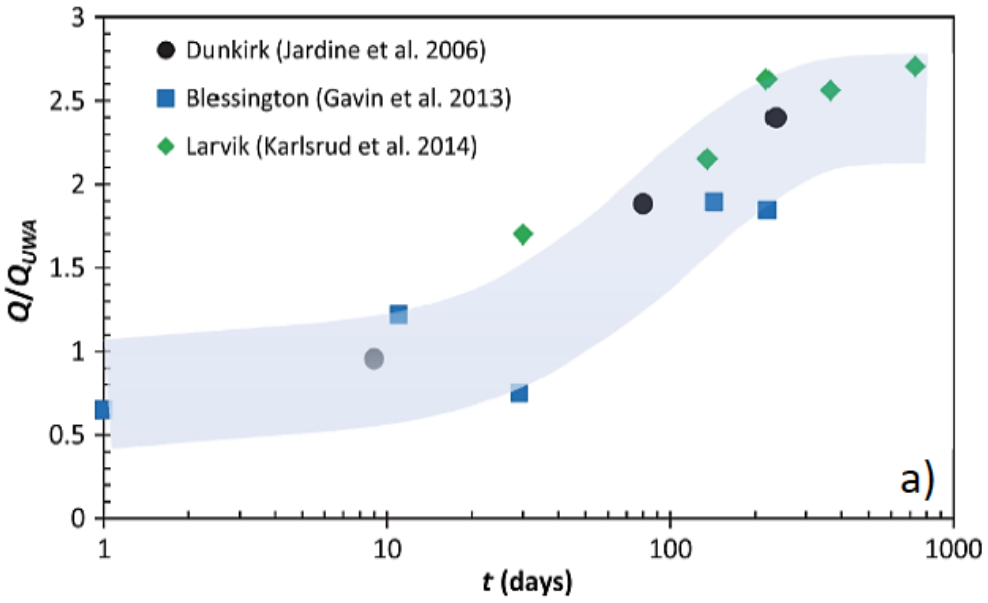

Figure 1. Graph showing current data on pile ageing (Bittar et al. 2020). The y-axis shows the ratio of the pile capacity to the pile capacity estimate using the UWA method.

3.4 t-z Curves

The t-z curves describe the load transfer in friction along the shaft of the pile. The t-z curves for both sand and clay that are specified in the API code were used and referred to as the "API t-z curves".

Recent monitoring of offshore wind turbines installations suggests that the foundation is often stiffer than what is modeled in design (e.g., Skau et al. 2018). One hypothesis is that the pile models may not be accurately capturing the stress-strain response of the soil in the lower strain levels. Therefore, as part of this study, the t-z curves by Kraft et al. (1981) were also utilized. These curves were developed by integration of shear strain in the radial direction assuming a constant soil shear modulus (Randolph and Wroth 1978). At low pile load or displacement levels the soil modulus is equal to G_0. The curves are then modified for larger strains assuming a hyperbolic load-displacement relationship up to the maximum shaft friction as defined by the following equation:

$$w = \frac{\tau r_0}{G_0} \ln \left[\frac{r_m - \frac{\tau R_f}{\tau_{max}}}{\frac{r_0}{1 - \frac{\tau R_f}{\tau_{max}}}} \right] \quad (3)$$

where w=axial displacement, τ=pile shaft shear stress, r_0=pile radius, G_0=small strain shear modulus, r_m="magical" radius, and R_f=curve fitting parameter typically taken as 0.9 for most conditions. The magical radius defines the radial distance at which the strains become negligible and is defined by the following (Kraft et al. 1981):

$$r_m = 2L\rho(1-\upsilon) \quad (4)$$

where L=pile embedment length, ρ=ratio of G_0 at the pile toe to the value of G_0 located halfway down the pile, υ=Poisson's ratio. A value of ρ of 0.67 was used in the analysis that was obtained

from fitting a linear trend line to the G_0 data estimated from the CPT correlations as shown in Figure 2.

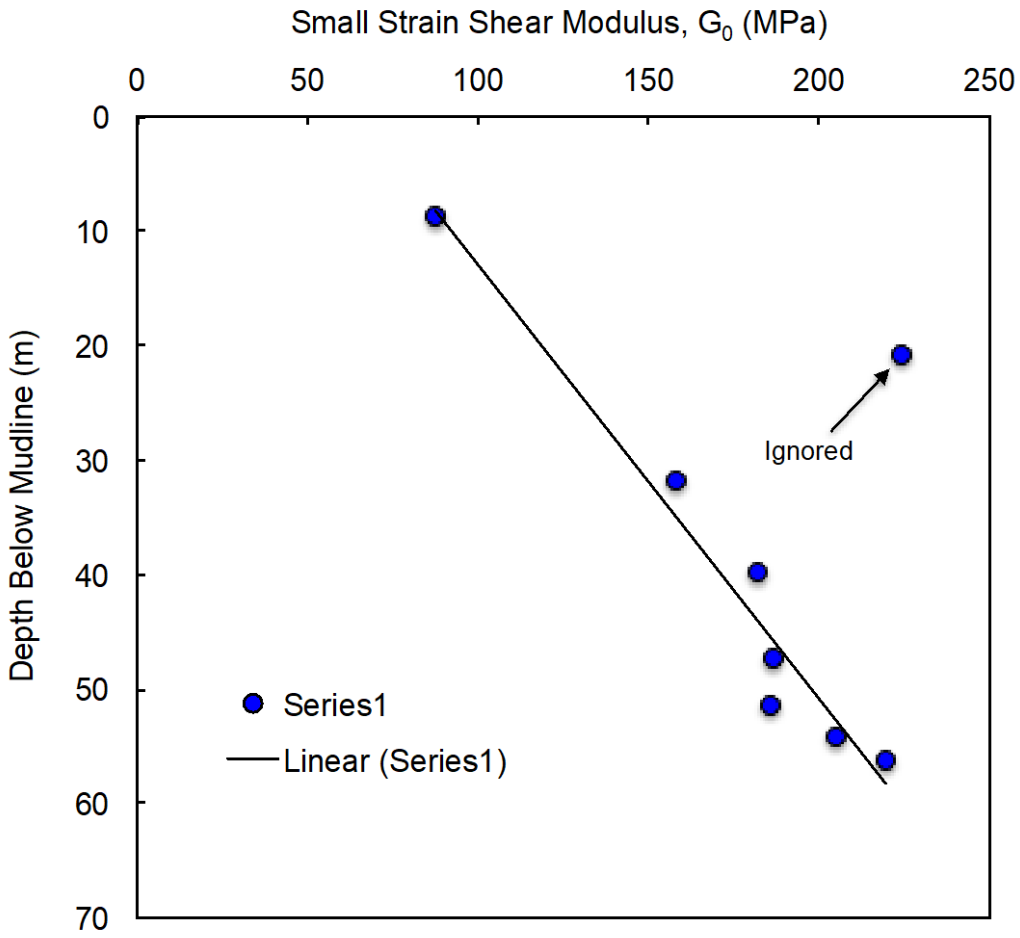

Figure 2. Depth profile of small strain shear modulus obtained using CPT correlations. A linear trendline was also fit to the data and used as a basis for developing parameters for the pile analysis.

Cyclic loading can affect pile capacity, stiffness, and permanent deformations. The API code suggests that use of standard static capacity methods combined with commonly accepted factors of safety to some degree account for the effects of cyclic loading. Moreover, the recent BOEM-sponsored research on axially loaded piles (e.g. Rahim et al. 2020) suggest that ageing, which is not typically included in design, provides an additional margin of safety against cyclic degradation of capacity. Consistent with the approach used to design the platform, cyclic effects on axial capacity and deformation were not explicitly modeled.

3.5 q-z Curve

The q-z curves describe the axial resistance at the toe. The q-z curves for both sand and clay that are specified in the API code were used in all analysis cases and referred to as “API” q-z curves.

3.6 p-y Curves

The p-y curves describe the lateral soil resistance. The API RP 2A p-y curves for sand (called “API Sand”) were used for the sand layers, along with Reese et al. (1975) for the stiff clay layers.

3.7 Pile Head Boundary Conditions

As the jacket structure is loaded laterally it will simultaneously subject the pile head to a combination of axial, lateral, and moment loads. Since the magnitudes and even relative proportions of these loads are unknown, some simplifying assumptions must be made in the pile model about the boundary conditions at the pile head to numerically construct the load-displacement curves for the pile head.

The first assumption is that the pile head cannot rotate and thus is considered a fixed-headed condition. Some rotation would be expected but it is anticipated that it would be very small and would have minimal effect on the vertical stiffness.

For vertical loading the boundary conditions for the pile head in the x and y directions must be specified. Since the true horizontal loads and/or displacements are unknown, two conditions were considered. In the first condition, the pile head was free to translate in both the x and y directions. In the second condition, the pile head was restrained from translation in both the x and y directions. Both conditions are explored in the analysis to assess their sensitivity.

For the horizontal loading in one direction (e.g., x), the vertical load is unknown and thus the boundary conditions in the orthogonal direction (e.g., y) need to be specified. Both the restrained and unrestrained conditions were investigated.

3.8 Analysis Cases

A summary of the analysis cases is provided in Table 3.

Table 3. Soil models used in soil structure interaction analysis. The pile head conditions for all cases are assumed to be "fixed-headed" (i.e. fixed against rotation).

Case	Static Capacity Method	t-z sand	t-z clay	q-z sand	p-y sand	p-y clay	Pile Head Restraint
Case 1A	API	API	API	API	API RP 2A (static)	Reese et al. 1975 (static)	R
Case 1B	API	API	API	API	API RP 2A (static)	Reese et al. 1975 (static)	UR
Case 1C	API	API	API	API	API RP 2A (cyclic)	Reese et al. 1975 (cyclic)	UR
Case 2A	UWA	Kraft et al. (1982)	Kraft et al. (1982)	API	API RP 2A (static)	Reese et al. 1975 (static)	R
Case 2B	UWA w/ ageing	Kraft et al. (1982)	Kraft et al. (1982)	API	API RP 2A (static)	Reese et al. 1975 (static)	R

Note: R=restrained from translation in a direction orthogonal to the loading direction, UR-unrestrained from translation in a direction orthogonal to the loading direction.

Case 1 was consistent with the "Main Text" API method.

Case 2 utilized API p-y curves but used different t-z curves and ultimate shaft resistance methods. Case 2A used the UWA-05 method for ultimate unit shaft resistance and Kraft et al. (1981) for t-z response based on the small strain shear modulus. Case 2B investigated the effects of ageing by doubling the ultimate unit shaft resistance based on Figure 1. Although ageing can also affect the small strain shear modulus, the axial stiffness of large diameter piles is mainly dominated by the strains in the soil outside the interface shear band, which is minimally disturbed during pile installation. Therefore, it is presumed that ageing would occur within the interface shear band, but would likely not contribute significantly to the axial stiffness of the pile.

4.0 PUSHOVER ANALYSIS RESULTS AND DISCUSSION

4.1 Horizontal Loading

Horizontal load-displacement analyses were only performed using Case 1 soil models. The horizontal load-displacement curves are shown in Figure 3.

The effect of the boundary conditions under horizontal loading was assessed through comparison of Cases 1A and 1B. Restraining pile head translation in a direction that is perpendicular to the loading direction had a stiffness that was up to about 25% higher than the unrestrained case in the "Out" direction, and up to 3 times higher in the "In" direction (see load orientation on Figure 5).

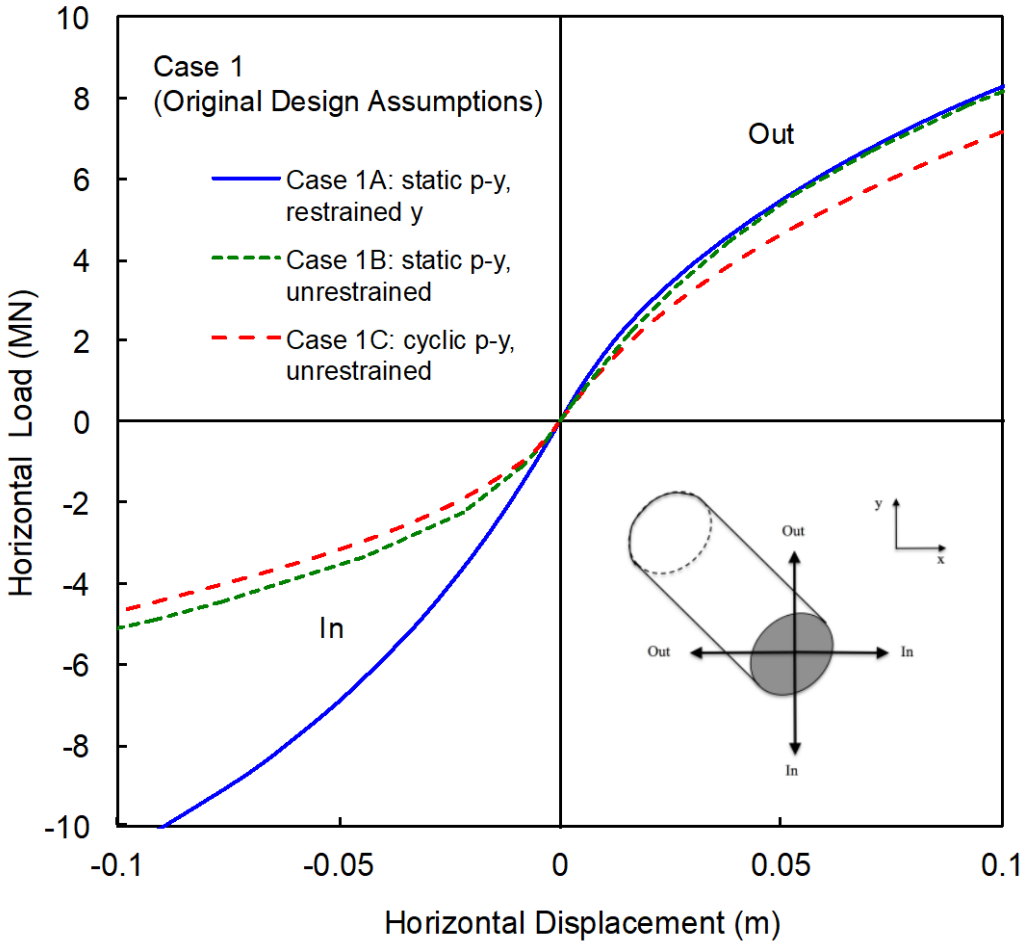

Figure 3. Case 1 horizontal load-displacement curve developed from the static pushover analysis.

The effect of using static versus cyclic p-y curves under horizontal loading was assessed through comparison of Cases 1B and 1C for unrestrained conditions. A comparison of Case 1B and 1C indicates that the stiffness calculated with the static p-y curves was about 28% higher than was calculated using the cyclic p-y curves.

4.2 Vertical Loading

Vertical load-displacement analyses were performed using both Case 1 and Case 2 soil models. The vertical load-displacement curves are shown in Figure 4.

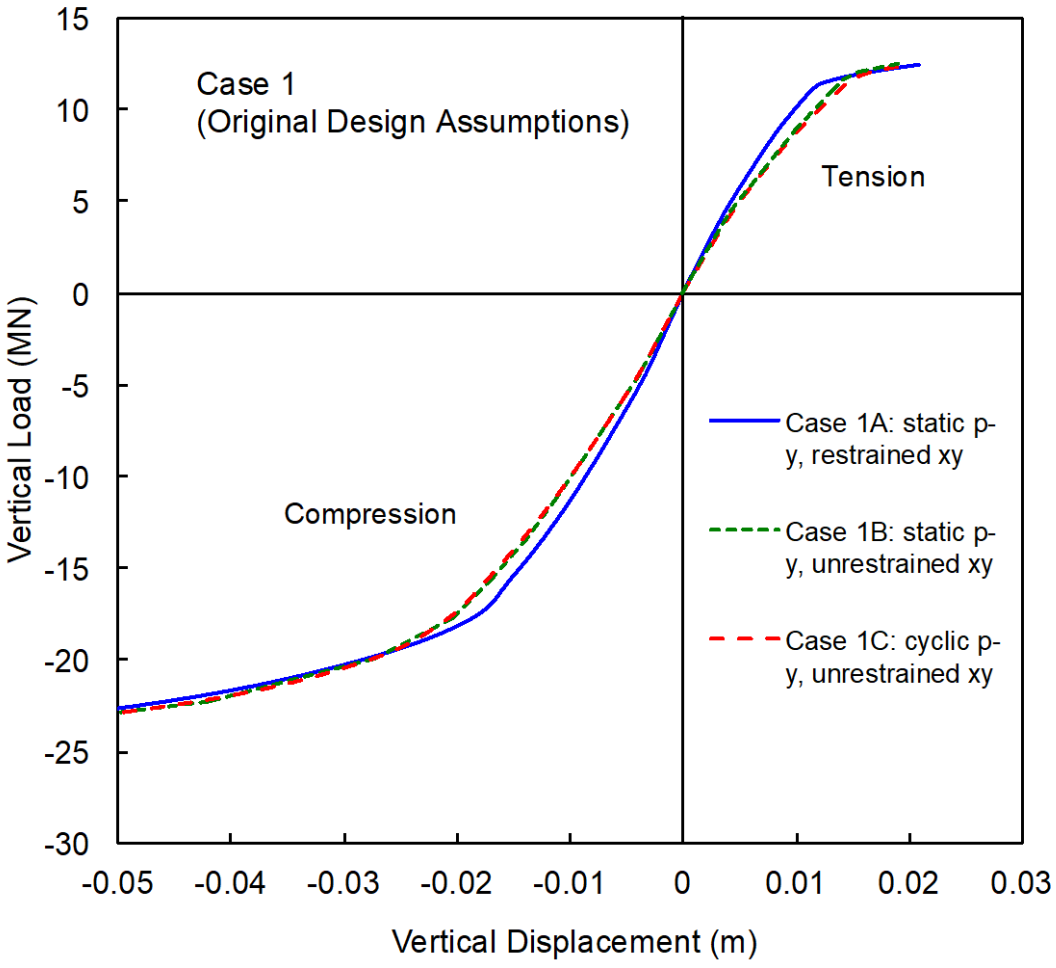

Figure 4. Case 1 vertical load-displacement curves developed from the static pushover analysis.

Case 1 was used to assess the sensitivity of the pile head boundary conditions on the vertical response. Case 1A is for restrained in x and y and Case 1B is unrestrained in x and y. As shown in Figure 4, the stiffness in the restrained case (1A) was up to 18% stiffer higher than the unrestrained case (1B) with the difference being most significant at the lower load levels. The results of case 1B were also comparable to the results if the pile was assumed to be vertical.

Case 1B and 1C were used to investigate the use of static vs. cyclic p-y curves on the vertical pile head response. Case 1B uses the static p-y curves and Case 1C uses the cyclic p-y curves and in both cases the pile is unrestrained in the x and y directions. Given that the piles are almost vertical it anticipated that the p-y response would not have much of an influence. As shown in Figure 4 there was negligible difference between the two cases.

Case 2 and Case 1A were compared by assuming that the pile head was vertically loaded and restrained in both the x and y directions. This was chosen over the unrestrained case as the jacket likely provides some horizontal restraint. Also, since the p-y curves had little effect on the vertical pile head response, only the static p-y curves were used. The load-displacement curves are shown in Figure 5. As shown in Figure 5 the pile resistance at high load levels were somewhat consistent between Case 1A (API) and Case 2A (UWA and Kraft t-z). However, Case 2B (UWA aged and Kraft t-z) had a much higher axial resistance at high load levels. Case 2 was clearly stiffer at the lower load levels most likely because of incorporation of G_0 into the t-z model.

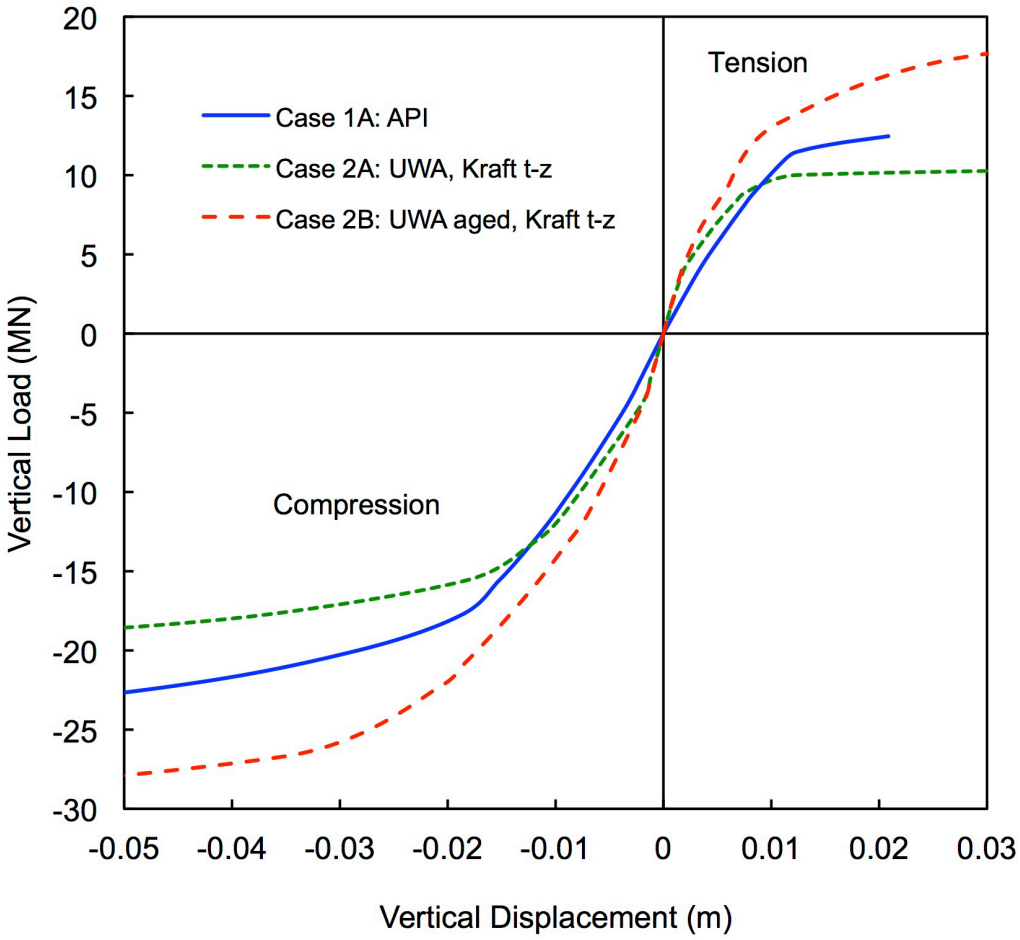

Figure 5. Case 1A and Case 2 vertical load-displacement curves developed from the static pushover analysis.

5.0 FOUNDATION SPRING CONSTANTS

The vertical load-displacement "backbone" curves developed in the static pushover analysis above were used as a basis for defining best estimates of the spring constants for a simple equivalent linear spring foundation model. Since the behavior is nonlinear it is important to select the secant stiffness that is consistent with the anticipated cyclic load levels being applied to the foundation. Only vertical spring constants are defined in this section, but lateral spring constants could also be derived from Figure 3 if they are needed.

The load that is applied to the pile will have both a mean (or static) component as well as a cyclic component. Based on typical Masing behavior, an equivalent linear vertical stiffness was determined by taking the slope from the origin to any specified point on the static backbone curves shown in Figure 5. Figure 6 plots the equivalent linear vertical stiffness versus the applied vertical load both in the compressive and tensile loading directions. The results reflect the non-linear behavior of the soil; the foundation stiffness is highest at an applied load of zero, and decreases with an increase in load level.

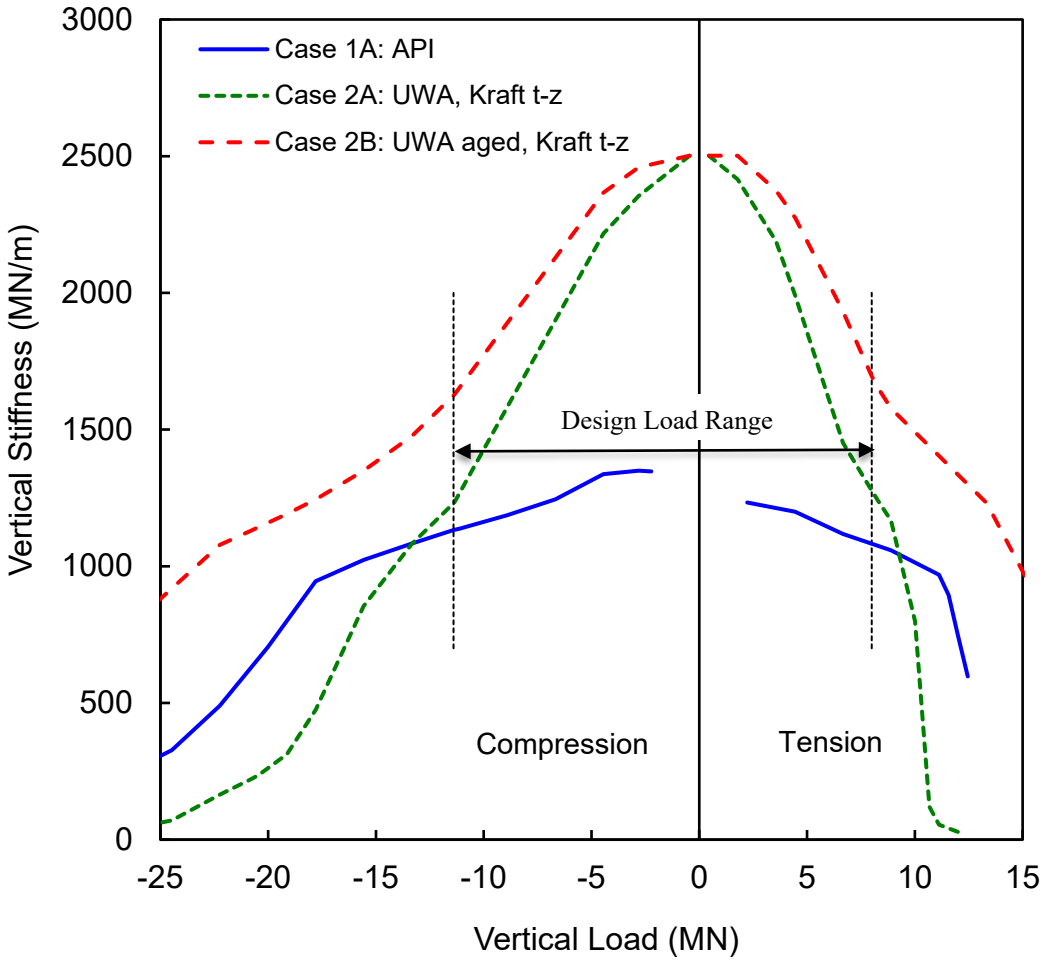

Figure 6. Vertical stiffness calculated from the load-displacement curves developed from the static pushover analysis.

To bound the range of possible vertical stiffness values, maximum and minimum values were selected from Figure 6 within the anticipated working load range. The load range was based on

information provided in a preliminary geotechnical report. The upper and lower bound values of vertical stiffness are summarized in Table 4 and range from about 1,080 to 2,500 MN/m.

Table 4. Summary of lower and upper bound vertical stiffness parameters within the maximum design load ranges indicated in GZA (2010).

	Vertical Stiffness (MN/m)	
Case	Lower Bound	Upper Bound
Case 1A	1080	1350
Case 2A	1230	2500
Case 2B	1630	2500

The analytical solutions for axial pile behavior derived by Randolph and Wroth (1978) were also used as an independent check on the numerical results. The model assumes a vertical pile embedded in an elastic material and the toe resistance is neglected. The model assumes a Gibson soil where the stiffness is either constant or linearly increasing with depth. Based on the G_0 profile shown in Figure 2, the analytical result was 2,380 MN/m. This was consistent with the Case 2 results at low load levels or displacements that also utilize G_0 in the t-z model formulation.

6.0 REFERENCES

Bittar, E., Lehane, B., Watson, P., and Deeks, A. (2020). "Effect of Cyclic History on the Ageing of Shaft Friction of Driven Piles in Sand." *Proceedings of the 2020 ISFOG Conference* (in press).

Rahim, A., Deeks, A., Bradshaw, A.S., Keefe, T., Hussein, A., Schneider, J. (2020). *Additional Model Testing of Cyclic Axial Loading of Piles for Jacket Foundations.* Draft Final Report Rev. No. 3 dated 8/20/20. Submitted to BOEM, Contract Number 140M0118C002.

Kraft, L. M., Ray, R. P., and Kagawa, T. (1981). "Theoretical t-z curves," *Journal of the Geotechnical Engineering Division*, Proceedings Paper 16653, American Society of Civil Engineers, Vol 107(GT11).

Lehane, B., Schneider, J., & Xu, X. (2005). "The UWA-05 method for prediction of axial capacity of driven piles in sand. In M. J. Cassidy, & S. Gourvenec (Eds.)", *Proceedings of the International Symposium on Frontiers in Offshore Geotechnics* (Perth, Australia ed., Vol. n/a, pp. 683-689). CRC Press/Balkema

Mayne, P.W. and Rix, G.J. (1993). "Gmax-qc relationship for clays." *Geotechnical Testing Journal*, 16(1), 54-60.

Randolph, M.F., and Wroth, P.C. (1978). "Analysis of deformation of vertically loaded piles." *Journal of the Geotechnical Engineering Division*, ASCE 104(GT12), 1465-1487.

Reese, L. C., and Welch, R. C. (1975). "Lateral loading of deep foundations in stiff clay," *Journal of the Geotechnical Engineering Division*, ASCE 101(GT7), 633-649.

Rix, G.J. and Stokoe, K.H. (1991). "Correlation of initial tangent modulus and cone penetration resistance", *Calibration Chamber Testing*, International Symposium on Calibration Testing, Elsevier publishing, New York, 351-362.

Skau, K.S., Page, A.M., Kaynia, A.M., Lovholt, F., Noren-Cosgriff, K., Sturm, H., Andersen, H.S., Nygard, T.A., Jostad, H.P, Eiksund, G., Havmoller, O., Strom, P., and Eichler, D. (2018) "REDWIN – REDucing cost in offshore WINd by integrated structural and geotechnical design." *Journal of Physics: Conference Series* 1104 012029
http://iopscience.iop.org/article/10.1088/1742-6596/1104/1/012